# Similarity of the Signatures of the Initial Stages of Phase Separation in Metastable and Unstable Polymer Blends

Amish J. Patel, Timothy J. Rappl, and Nitash P. Balsara

# Similarity of the Signatures of the Initial Stages of Phase Separation in Metastable and Unstable Polymer Blends

Amish J. Patel,[1] Timothy J. Rappl,[1] and Nitash P. Balsara[1,2,*]

[1]*Department of Chemical Engineering, University of California, Berkeley, California 94720*
[2]*Materials Sciences Division and Environmental Energy Technologies Division,*
*Lawrence Berkeley National Laboratory, University of California, Berkeley, California 94720*

Time-resolved small angle neutron scattering was used to probe the initial stages of liquid-liquid phase separation in both, critical and off-critical binary polymer blends and the critical ($q_c$) and most probable ($q_m$) wave-vectors were identified for several quench depths. For the *critical* blend, the Cahn-Hilliard-Cook theory provides a framework for analyzing the data and explains the observed decrease in $q_m$ with time. For the *off-critical* blend, $q_m$ is independent of quench time, regardless of whether the quench is metastable or unstable.

The standard phase diagram of binary liquid mixtures contains two curves: the binodal curve which is the locus of the compositions of the coexisting phases and the spinodal curve which is the thermodynamic limit of the stability of the homogeneous phase. According to classical treatments, the transformation of a homogeneous binary liquid into a phase separated mixture after a quench from the single phase region of the phase diagram to the two-phase region occurs by two mechanisms: nucleation and growth, which occurs if the quench lies between the binodal and the spinodal curves (the metastable region), and spinodal decomposition if the quench lies within the spinodal curve (the unstable region) [1–3]. However, subsequent theoretical treatments that have examined the crossover from nucleation to spinodal decomposition suggest that the situation may be more complex [4, 5].

In this letter, we present time-resolved small angle neutron scattering (SANS) data from two polymer blends that are quenched from the one-phase to the two-phase region: a critical blend that is quenched directly into the unstable region and an off-critical blend quenched to various quench depths, both in the metastable and the unstable regions. The data were obtained during the initial stages of phase separation, before coarsening sets in. SANS results from both the blends have been presented in two separate papers [6, 7]. The main purpose of this letter is to combine the data presented in these two papers to illustrate that: 1) For the off-critical blend, there are no qualitative differences between quenches in the metastable and unstable regions. 2) Quenches for the critical and off-critical blends display differences in the time evolution of the most probable wave-vector. This raises questions concerning the role of the spinodal in demarcating distinct phase separation mechanisms.

Both polymer blends are made up of high molecular weight liquid polyolefins: deuterated polymethylbutylene (*d*PMB) and hydrogenous polyethylbutylene (*h*PEB). The methods used to synthesize and characterize these nearly-monodisperse homopolymers are described in ref. [8]. The weight-average molecular weights, $M_w$, of the polymers that constitute the off-critical blend are 153 kg/mol (*d*PMB) and 197 kg/mol (*h*PEB). The radii of gyration, $R_g$, of both chains are $15.4 \pm 1.0$ nm. The results reported here are for a blend with *d*PMB volume fraction, $\phi_{d\mathrm{PMB}} = 0.20$. For the critical blend, $M_w$ of the polymers are 153 kg/mol (*d*PMB) and 131 kg/mol (*h*PEB) and $R_g$ of both chains are $14.0 \pm 1.0$ nm. The critical composition, based on the Flory-Huggins theory [9, 10], is $\phi_{d\mathrm{PMB}} = 0.493$. All polymers are highly entangled, resulting in extremely slow phase separation, which can be tracked by time-resolved SANS.

The azimuthally averaged coherent scattering intensity, $I$, as a function of the magnitude of the scattering vector, $q$, was obtained by methods reported in ref. [8]. Static SANS enabled the thermodynamic characterization of our system, while time-resolved SANS enabled the study of the early stages of phase separation. We use the Flory-Huggins theory to quantify the thermodynamic properties of our blends. The $T$ and $P$ dependence of the Flory-Huggins interaction parameter, $\chi$, for the system of interest and the phase diagrams of the blends used in this paper have been reported previously [6–8]. We define the quench depth, $\kappa(T, P) = \chi(T, P)/\chi_b - 1$, where $\chi_b$ is the value of $\chi$ at the binodal. In Table 1, we list the final $T$ and $P$ of the quenches as well as the corresponding $\kappa$-values, for both critical and off-critical blends.

TABLE I: Experimental conditions and quench depths

| $T(^\circ C)$ | $P$(kbar) | $\kappa$ | $T(^\circ C)$ | $P$(kbar) | $\kappa$ |
|---|---|---|---|---|---|
| Critical blend | | | Off-critical blend | | |
| 70 | 1.24 | 0.04 | 59 | 1.52 | 0.26 |
| 70 | 1.66 | 0.09 | 59 | 1.72 | 0.30 |
| 70 | 2.07 | 0.15 | 59 | 2.00 | 0.34 |
| 70 | 2.48 | 0.20 | 59 | 2.34 | 0.40 |
| Off-critical blend | | | 59 | 2.69 | 0.46 |
| 59 | 0.90 | 0.16 | 59 | 3.03 | 0.52 |
| 59 | 1.10 | 0.19 | 49 | 2.69 | 0.59 |
| 59 | 1.31 | 0.23 | 40 | 2.69 | 0.73 |

In Figure 1, we show the calculated binodal curves for both the critical and off-critical blends, as well as
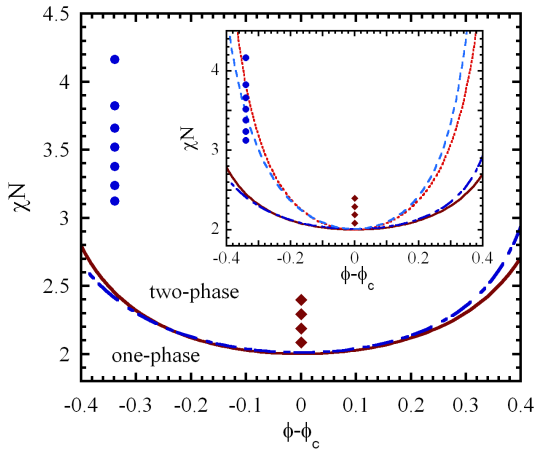
FIG. 1: Binodal curves for the critical (in red) as well as the off-critical (in blue) blend are shown along with the locations of the various quenches studied. Inset shows the full phase diagram with both the binodal and the spinodal curves.

the locations of the quenches that were investigated. [$N = \sqrt{N_1 N_2}$ and $\phi_c$ is the critical composition; $N_i$ is the number of monomers per chain for each polymer, based on a 0.1 nm$^3$ reference volume.] The locations of the quenches relative to the mean-field spinodal curves are shown in the inset of Figure 1.

Typical data obtained from the off-critical blend are shown in Fig. 2a, where we show the SANS profiles during a quench from the one-phase region to 2.34 kbar and 59°C, which lies in the metastable region of the phase diagram. The arrow shows the location of the critical wave-vector, $q_c$. The SANS profiles are characterized by a rapid increase in $I(t)$ for $q$-values smaller than $q_c$ as well as the appearance of a peak in $I(q)$. In contrast, $I(q > q_c)$ does not change with time in the early stage of phase separation. We have argued that the size of the critical nucleus in the nucleation and growth regime is of order $1/q_c$ [11]. In Fig. 2b, we show SANS profiles for the off-critical blend during a quench to 2.69 kbar and 59°C, which lies in the unstable region of the phase diagram. There is no qualitative difference between the SANS profiles resulting from quenches in the metastable and unstable regions (compare Figures 2a and 2b). In the inset of Fig. 2b, we show the SANS profiles obtained from the critical blend during an unstable quench to 1.66 kbar and 70°C. The arrow shows the location of the critical wave-vector, $q_c$, obtained by well-established methods for analyzing data during spinodal decomposition [12]. Data similar to those shown in Figure 2 were obtained from the critical and off-critical blends at various quench depths by controlling the final $T$ and $P$.

In Fig. 3a, we show the position of the peak in $I(q)$, $q_m$, as a function of quench time for several quenches using the off-critical blend. There is no change (within experimental uncertainty) in $q_m$ as a function of quench time for quenches into the metastable as well as the unstable regions. The kinetics of phase separation of the
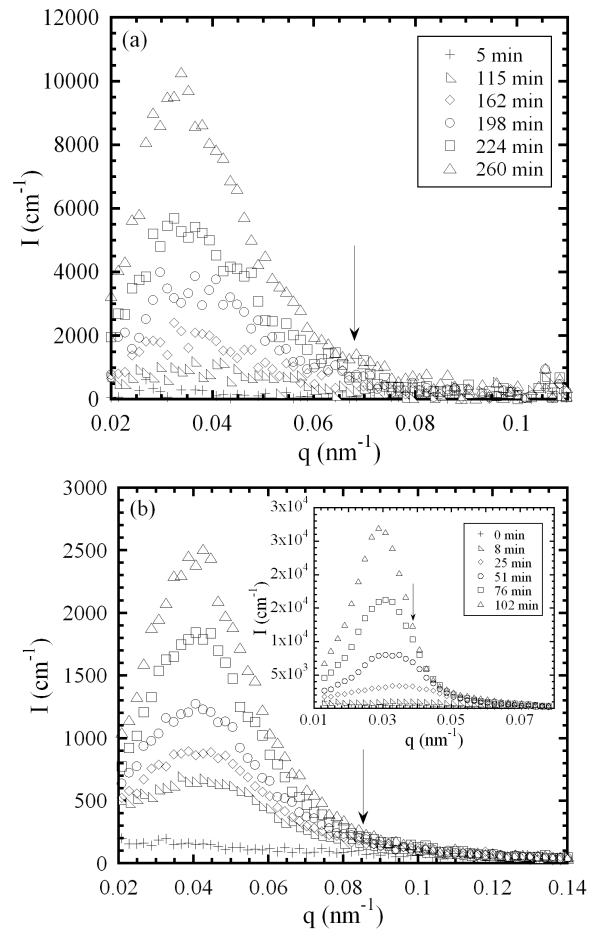


FIG. 2: Time-resolved SANS intensity, $I$ vs $q$ measured for the off-critical blend during the (a) 2.34 kbar (metastable) quench, and the (b) 2.69 kbar (unstable) quench (shown at $t = 3, 80, 102, 128, 154$ and $173$ min). Inset shows $I(q)$ for the critical blend during the 1.66 kbar quench. The arrows indicate the location of the critical wave-vector, $q_c$.

off-critical blend is thus governed by two characteristic wave vectors, $q_c$ and $q_p$; we take $q_p$ to be the average value of $q_m$ for each of the quenches shown in Fig. 3a. Quenches of the critical blend into the unstable region of the phase diagram also result in scattering profiles with peaks. However, in this case, $q_m$ decreases monotonically with time as shown in Fig. 3b.

The Cahn-Hilliard-Cook (CHC) theory predicts the time evolution of the scattering profile of unstable systems [12–15]: $I(q, t) = I_T(q) + [I_0(q) - I_T(q)] \exp[2R(q)t]$. In ref. [7], we showed that our measurements are in excellent agreement with the CHC equation, enabling the determination of $I_0(q)$, $I_T(q)$, and $R(q)$ for each of the quenches. This provides the basis for understanding the time evolution of $q_m$. At short times, $I(q, t) \approx I_0(q) + 2R(q)[I_0(q) - I_T(q)]t$. Hence, we expect a peak in $I(q)$ to emerge at the value of $q$, for which the initial rate of increase of $I(q, t)$, denoted by $J(q) = 2R(q)[I_0(q) - I_T(q)]$ is maximum. While $I_T(q)$ has a pole at $q = q_c$, $R(q_c) = 0$ and $J(q)$ is a contin-
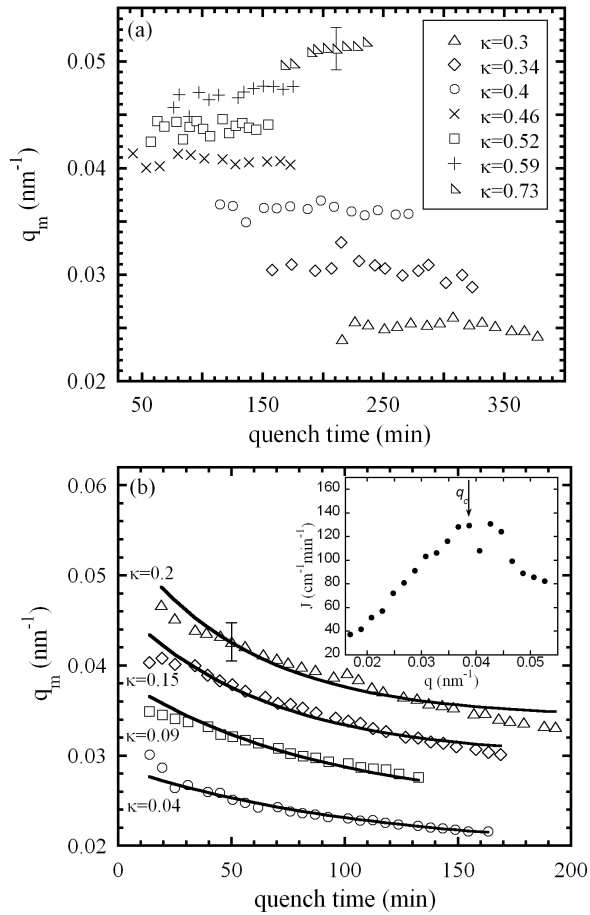
FIG. 3: SANS peak position, $q_m$, as a function of quench time for (a) off-critical and (b) critical blends. Solid curves are single-parameter exponential fits to the data with $\tau = 109$, 89, 65 and 56 min for $\kappa = 0.04$, 0.09, 0.15 and 0.2 respectively. The typical uncertainty in $q_m$ is also shown. Inset shows the initial rate of increase in the scattering intensity, $J(q)$, for the 1.66 kbar quench. The arrow indicates the location of $q_c$.

uous function of $q$. The pole at $q = q_c$ suggests the possibility of a maximum in $J(q)$ in the vicinity of $q_c$. This is indeed the case for all the quenches studied. We show $J(q)$ for the 1.66 kbar quench in the inset of Fig. 3b. There is good agreement between the location of the maximum in $J(q)$ and $q_c$, shown by an arrow. At long times, the exponent in the CHC equation governs the behavior of $I(q)$, resulting in a peak at a $q$-value, corresponding to the maximum in $R(q)$, which we call $q_p$. Thus $q_m(t = 0) \approx q_c$ and $q_m(t \to \infty) = q_p$. The simplest function that captures the evolution of $q_m(t)$ from $q_c$ to $q_p$ is: $q_m(t) = q_p + (q_c - q_p) \exp(-t/\tau)$. This functional form is used to fit the data from the critical blend using $\tau$ as the only adjustable parameter, and the fits are in good agreement with the data (Fig. 3b). As was the case for the off-critical blend, phase separation kinetics of the critical blend are also governed by two characteristic scattering vectors, $q_c$ and $q_p$. While the methodologies for determining $q_c$ and $q_p$ in critical and off-critical blends are different, the physical significance of the wave-

vectors is the same: $1/q_c$ represents the length scale of the smallest structures that grow during phase separation while $1/q_p$ represents the length scale that dominates the phase separated structure formed during the early stages.

Thus, the CHC theory provides a framework for analyzing $I(q, t)$ from critical blends, and explains the decrease in $q_m$. However, there is no framework for analyzing time-resolved scattering data from nucleating blends. While we do not have a theoretical basis for the time invariance of $q_m$ for off-critical quenches, a possible explanation might be that $q_m$ represents the average distance between nucleating centers that does not change as the nuclei grow during the early stages of phase separation.

In Figures 4a and 4b, we plot $q_p R_g$ and $q_c R_g$ as a function of the quench depth, $\kappa$, for the critical and off-critical blends. The dependences of both characteristic wave-vectors on quench depth are similar for the critical and off-critical blend except for the fact that the off-critical data are shifted to the right along the $\kappa$-axis.
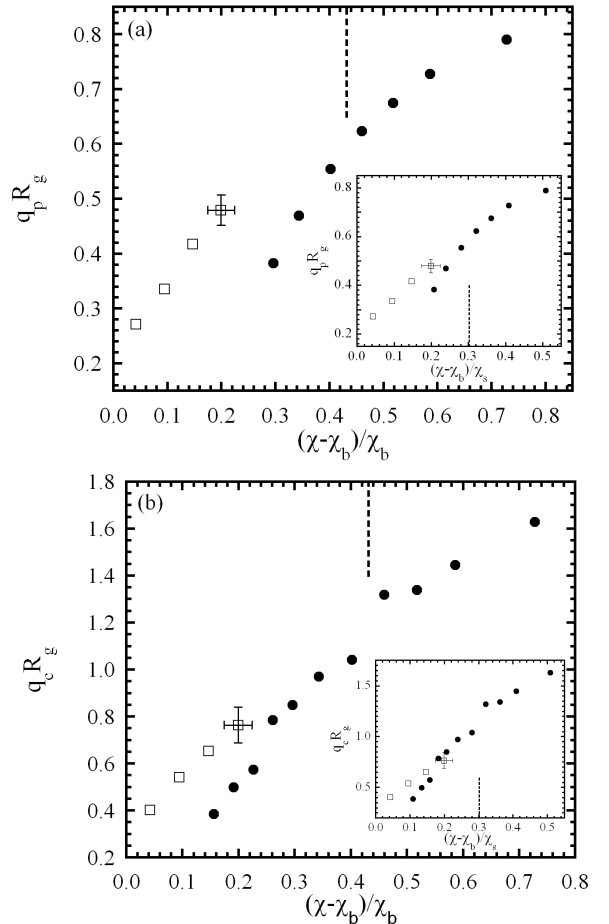


FIG. 4: Dimensionless characteristic wave-vectors, (a) $q_m$, and (b) $q_c$ as a function of the quench depth, $(\chi - \chi_b)/\chi_b$ for the critical (open squares) and off-critical (filled circles) blends. The insets show $q_m$ and $q_c$ as a function of an alternative definition of quench depth $(\chi - \chi_b)/\chi_s$. The dashed lines mark the position of the spinodal for the off-critical blend. Typical uncertainties are also shown.

The shift is larger in the $q_p R_g$ versus $\kappa$ plot. In the insets of Figures 4a and 4b, we show the same data plotted versus $\kappa_s = (\chi - \chi_b)/\chi_s$, where $\chi_s$ is the value of $\chi$ at the spinodal. The distinction between critical and off-critical systems is significantly reduced when $\kappa_s$ is used to define quench depth.

The data in Figures 2 and 4 indicate that the qualitative features of the scattering profiles obtained during the initial stages of phase separation are independent of quench depth. While the spinodal may help in organizing the data as we have shown in the insets of Fig. 4, it is does not demarcate different mechanistic regimes. Theoretical work of Binder and Stauffer [16] showed that the characteristic length-scale of phase separation in mixtures of low molecular weight compounds was unaffected by the presence of the spinodal. It was argued that the spinodal, a mean-field concept, is destroyed by concentration fluctuations. Anticipation that the spinodal curve and mean-field behavior would be recovered in polymer blends was based on the scaling arguments of de Gennes, who showed that the Ginzburg Number, $Gi$, which quantifies the importance of fluctuations, follows a $Gi \sim 1/N$ scaling law [17]. More refined calculations by Wang [18] indicate that while this scaling law is correct in the large $N$ limit, it is not obeyed for blends with $N < 10^4$. For $Gi$ to be significantly smaller than unity (say 0.01), the values of $N$ required are of order $10^4$ for $\phi = 0.5$, corresponding to component $M_w \sim 10^3$ kg/mol. While experiments on such large systems may one day be carried out, they represent a small portion of parameter space with virtually no practical significance. There are thus compelling reasons for eliminating the spinodal curve from the reported phase diagrams of binary mixtures that undergo liquid-liquid phase separation as we have done in Figure 1.

Additionally, theoretical studies that improve upon the Cahn-Hilliard treatment by using a non-linear local free energy [4, 5] report that there is no change in the mechanism of phase separation on crossing the spinodal. Novick-Cohen uses a quartic free energy expression and reports that a parameter $B$, which is related to the higher derivatives of the free energy, governs the mechanism of phase separation [4]. The non-linear theory predicts a crossover inside the spinodal from a nucleation-like mechanism near the spinodal ($B >> 1$) to classical spinodal decomposition, deep within the spinodal ($B << 1$). It can be shown that for a Flory-Huggins blend, $B \approx 4.5\sqrt{(\chi_s - \chi_b)/|\chi - \chi_s|}$. For the critical blend, $\chi_b = \chi_s \implies B = 0$ and thus classical spinodal decomposition is observed. For the off-critical blend studied in this letter, the lowest value of $B$ was 5.2, i.e. the $B << 1$ criterion was never reached and thus only the nucleation-like mechanism was observed.

In conclusion, we have found similarities in the time-resolved scattering signatures of the initial stages of phase separation, with peaks observed in $I(q)$ for all quenches and for both the critical and the off-critical polymer blends (Fig. 2). However, there are subtle differences, specifically in the evolution of $q_m$ with quench time (Fig. 3). For critical quenches, the CHC theory explains the observed decrease in $q_m$ with time. In contrast, for the off-critical blend, $q_m$ is independent of quench time, regardless of whether the quench is metastable or unstable. The difference between critical and off-critical quenches as well as the similarities between metastable and unstable off-critical quenches can be explained in the context of theories that incorporate non-linear effects into the Cahn-Hilliard analysis. However, a theoretical framework for describing $I(q, t)$ for nucleating blends, akin to the CHC theory for critical quenches, is still missing. We hope that the data in Figures 3 and 4 will guide the development of such a framework.

———————

* Electronic address: nbalsara@berkeley.edu

[1] J. W. Gibbs, *The Scientific Papers of J. Willard Gibbs* (Dover, New York, 1961).

[2] J. W. Cahn, J. Chem. Phys. **42**, 93 (1965).

[3] J. W. Cahn and J. E. Hilliard, J. Chem. Phys. **31**, 688 (1959).

[4] A. Novick-Cohen, J. Stat. Phys. **38**, 707 (1985).

[5] U. Thiele, M. G. Velarde, and K. Neuffer, Phys. Rev. Lett. **87**, 016104 (2001).

[6] A. J. Patel and N. P. Balsara, Macromolecules **40**, 1675 (2007).

[7] T. J. Rappl and N. P. Balsara, J. Chem. Phys. **122**, 214903 (2005).

[8] N. P. Balsara, S. V. Jonnalagadda, C. C. Lin, C. C. Han, and R. Krishnamoorti, J. Chem. Phys. **99**, 10011 (1993).

[9] P. J. Flory, J. Chem. Phys. **10** (1942).

[10] M. L. Huggins, J. Phys. Chem. **46** (1942).

[11] A. C. Pan, T. J. Rappl, D. Chandler, and N. P. Balsara, J. Phys. Chem. B **110**, 3692 (2006).

[12] H. E. Cook, Acta Metall. **18**, 297 (1970).

[13] K. Binder, J. Chem. Phys. **79**, 6387 (1983).

[14] F. S. Bates and P. Wiltzius, J. Chem. Phys. **91**, 3258 (1989).

[15] H. Jinnai, H. Hasegawa, T. Hashimoto, and C. C. Han, J. Chem. Phys. **99**, 4845 (1993).

[16] K. Binder and D. Stauffer, Phys. Rev. Lett. **33**, 1006 (1974).

[17] P. G. de Gennes, *Scaling Concepts in Polymer Physics* (Cornell University Press, Ithaca, NY, 1979).

[18] Z.-G. Wang, J. Chem. Phys. **117**, 481 (2002).